2014-04

Depression of the Normal-Superfluid Transition Temperature in Gated Bilayer Graphene

UTD AUTHOR(S): Massimo V. Fischetti

Depression of the normal-superfluid transition temperature in gated bilayer graphene

Massimo V. Fischetti[a)]
Department of Materials Science and Engineering, The University of Texas at Dallas, 800 W Campbell Rd. RL10, Richardson, Texas 75080, USA

(Received 7 March 2014; accepted 16 April 2014; published online 30 April 2014)

It is shown that the normal-superfluid transition in bilayer graphene predicted to occur at a high temperature is strongly affected not only by the dielectric constants of the substrate, interlayer, and gate insulators but also by the proximity of ideal metal gates. Even assuming optimistically a completely unscreened interlayer Coulomb interaction—thus bypassing the controversial problems regarding the proper way to screen the interlayer Coulomb interactions—it is shown that employing a gate-insulator thickness smaller than about 2-to-5 nm of equivalent SiO_2-thickness pushes the transition temperature significantly below 300 K to the 1 K–1 mK range, depending on the dielectric constant of the gate insulator and on the dielectric mismatch of the insulators employed. These results imply that thicker and low-dielectric-constant gate insulators should be employed to observe the phase transition, but exploiting the superfluid state of gated graphene-bilayers in room-temperature device applications may be challenging. © *2014 AIP Publishing LLC*. [http://dx.doi.org/10.1063/1.4873637]

I. INTRODUCTION

The theoretical prediction that a phase transition from a normal to a superfluid state in bilayer graphene (BLG) should occur at high temperatures[1–3] has triggered interest motivated not only by the scientific importance of such a transition but also by its promise of new technological applications. The possibility of designing high performance, low-power electronic devices that could exploit the properties of the superfluid state is illustrated by the bilayer pseudospin field-effect transistors (BiSFETs) proposed by Banerjee and coworkers[4] (Here "pseudospin" refers to the "which layer" degree of freedom that plays a role analogous to spin in the Bardeen-Cooper-Schrieffer (BCS) theory of superconductivity.).

Unfortunately, some confusion remains about the role that dielectric screening—dynamic or static, in the normal or superfluid state—plays in determining the transition temperature.[5–9] The situation has been summarized by Abergel *et al.*:[10] Given the difficulty of accounting for the dielectric response of free carriers or excitons in such a broken symmetry gapped system, they conclude that the "truth" lies somewhere between the results obtained using static screening—predicting a normal-superfluid transition temperature T_c smaller than $\sim 10^{-7}\, E_F/k_B$,[5,7] where E_F is the Fermi energy and k_B is the Boltzmann constant—and those obtained using the dynamically excitonic-state-screened interaction, $k_B T_c \sim 0.1\, E_F$,[9] in agreement with the original predictions.[1–3] An additional upper bound to the transition temperature is set by the Berezinski-Kosterlitz-Thouless temperature, T_{BKT}, above which thermally generated topological defects (mainly vortices) destroy the coherence. In Ref. 2, this is estimated to be $k_B T_{BKT} \sim E_F/8$ whereas the obvious upper bound $T_c < T_{BKT}$ is found in Ref. 7. Since here interest will be focused on even lower values for T_c, this issue will not be discussed further.

The difficulty of realizing an exciton condensation at room-temperature has been argued to originate from the basic fact that the linear dispersion in graphene renders the system weakly interacting.[11] Additional arguments supporting the lack of this experimental evidence in real systems have been presented by Abergel *et al.*:[10,12] Employing interactions statically screened in the normal state, they have shown that the effect of density fluctuations and charge unbalance in the two layers,[10] together with disorder,[12] may be responsible for an additional reduction of the transition temperature. The possible negative effect of misalignment of the two layers has also been considered by Register *et al.*[13,14] These considerations may explain why Coulomb-drag experiments performed so far,[15,16] while uncovering interesting phenomena at low temperatures (less than about 50 K), have failed to show the sharp increase of the drag expected from the occurrence of a normal-superfluid phase transition.

The discussion outlined above has been based mostly on the idealized situation of a BLG embedded in a homogeneous dielectric medium described by a macroscopic dielectric constant ϵ. In practice, though, both in experiments aimed at observing the elusive phase transition, as well in the realization of the BiSFETs, a bias must be applied to least one of the two graphene single-layers (SLGs) in order to induce the charges required to form excitons. Moreover, despite attempts to use low-dielectric constant intercalants[17] and even air gaps[18] between the layers and also between the BLG and the substrate, most likely, different dielectrics will be required to support the BLG and keep the two layers separated. Most important, gates sufficiently close to provide the required high capacitance will have to be employed. The effect of an inhomogeneous dielectric environment (possibly with high-κ dielectrics) has been considered by Register,

a)Electronic mail: max.fischetti@utdallas.edu

Reddy *et al.*[13,14] who showed that a large dielectric mismatch may pose additional challenges to the realization of devices based on the superfluid state and that new device designs employing lower-κ and thicker dielectrics may be required. The effect of an inhomogeneous dielectric environment has been considered also in Refs. 19–22. In particular, Badalyan and Peeters[19,20] have shown that dynamic screening effects in such inhomogeneous situations can enhance the interlayer interaction beyond what could be expected from estimates made assuming an average dielectric constant. However, the effect of the proximity of metallic (or highly conductive) gates has never been considered in detail.

The purpose of this paper is to quantify and extend the qualitative results of Refs. 13 and 14, and show that, indeed, the proximity of such gates and the presence of insulators with different dielectric constants (here referred to as "dielectric mismatch") suppresses dramatically the normal-superfluid transition temperature because of the screening effect of the polarization charges of the metal and at the interfaces even under the optimistic scenario of completely unscreened Coulomb interactions. In particular, it is shown that in single-gate structures gate dielectrics thinner than about 2-to-5 nm of equivalent SiO_2 thickness[23] (here denoted by t_{eq} and defined as $(\epsilon_{SiO_2}/\epsilon_{ins})\,t$, where t and ϵ_{ins} are the physical thickness and static dielectric constant of the insulator, respectively, and ϵ_{SiO_2} is the static dielectric constant of SiO_2) suppress the superfluid gap to values smaller than 1 meV, corresponding to transition temperatures of a few K. Therefore, air gaps and remote gates are required in order to observe the normal-superfluid transition, but the possibility of fabricating devices with the high gate capacitance required by the present scaling rules seems to be in serious doubt. These considerations are likely to apply also to hybrid double BLGs or SLG/BLG systems[24,25] as well as transition-metal dichalcogenides, since they are independent of the particular two-dimensional systems employed, at least when considering an unscreened interaction.

The paper is organized as follows: Section II reviews briefly the basic theory of the normal-superfluid transition and the gap equations that have to be solved to estimate the transition temperature. While these are well-known expressions, it is convenient to review them here explicitly in order to discuss their numerical solution. The Green's function of Poisson equation for a double-gated gated BLG is derived in Sec. III, also in its screened form (Sec. III B). Results are presented in Sec. IV, mainly for single-gated geometries (Sec. IV A), but also discussing briefly the effect of a double gate (Sec. IV B). Section IV C briefly discusses the effect of dynamic "un-gapped" screening also accounting for the dielectric response of the dielectrics and, finally, conclusions are drawn in Sec. V.

II. THE NORMAL-SUPERFLUID GAP IN BLG

A. Gap equation

The main quantity of interest here is the superfluid energy gap, $\Delta(k)$, that can be obtained form the Hamiltonian of BLG following the standard mean-field BCS approach. Assuming equal and opposite Fermi energies—so equal carrier densities—in the two SLGs, at zero temperature, the gap is given by the integral equation,

$$\Delta(\boldsymbol{k}) = \int \frac{\mathrm{d}\boldsymbol{k}'}{(2\pi)^2} \mathrm{eV}(\boldsymbol{k}-\boldsymbol{k}')\,\frac{1+\cos\phi}{2}\,\frac{\Delta(\boldsymbol{k}')}{2E(\boldsymbol{k}')}\,. \tag{1}$$

In this equation $E(\boldsymbol{k}) = \sqrt{\xi(\boldsymbol{k})^2 + \Delta(\boldsymbol{k})^2}$ is the energy of the quasi-particles, $\upsilon_F \approx 10^8\,\mathrm{cm/s}$ is the Fermi velocity in graphene, $\xi(\boldsymbol{k}) = \hbar\upsilon_F(k-k_F)$ is the kinetic energy of the free particles measured from the Fermi energy. As usual, k indicates the magnitude of the electrons and holes wave vectors measured from the Dirac point, k_F is the Fermi wave vector, and the factor $(1+\cos\phi)/2$ (where ϕ is the angle between $\boldsymbol{k}$ and $\boldsymbol{k}'$) is the overlap factor between the initial and final electronic states arising from the chirality of the electron and hole wavefunctions in SLG. Finally, $-eV(\boldsymbol{q})$ is the attractive Coulomb interlayer (exchange) interaction. In deriving this expression for the gap intervalley interlayer interactions are ignored, and the effect of intralayer Coulomb interactions can be absorbed into a small renormalization of the free kinetic energy $\xi(\boldsymbol{k})$ via a slightly different Fermi velocity,[26–28] effect that is also ignored. Finally, interlayer tunneling is neglected, so, usually a sufficiently large interlayer separation, $d = 1\,\mathrm{nm}$ or more, must be considered and results occasionally given for smaller interlayer separations should be regarded as "optimistic." Thanks to the isotropy of the electronic dispersion in graphene around the Dirac point, all quantities in the expression above depend only on the magnitude k of $\boldsymbol{k}$, and, in the following, the notation will be simplified accordingly.

The original predictions of a high transition temperature[1–3] were obtained using an unscreened interlayer interaction potential eV. In the ideal case of two SLGs separated by a distance d and embedded in a uniform dielectric medium with dielectric constant ϵ, the potential is simply $eV(q) = e^2/(2\epsilon q)e^{-qd}$. Kharitonov and Efetov[5] have shown that it possible to account for the screening effects due to the polarization of the free carriers in each graphene layer by treating the polarizability in an random-phase-approximation (RPA)-like approximation whose validity stems from the many "flavors" (spin, valley, and which-layer degeneracy) of the screening carriers.[5,7] Sodemann *et al.*[9] have later accounted for dynamic effects along the complex axis $i\omega$ (see Sec. IV C below), and have expressed the dynamically screened gap as a self-energy in the form of a Dyson equation,[9]

$$\Delta(k,i\omega) = \int \frac{\mathrm{d}\boldsymbol{k}'}{(2\pi)^2}\,\frac{1+\cos\phi}{2} \times \int_0^\infty \frac{\mathrm{d}(\hbar\omega')}{\pi}\,\frac{\Delta(k',i\omega')\,eV^{(\mathrm{RPA})}[|\boldsymbol{k}-\boldsymbol{k}'|,i(\omega-\omega')]}{\hbar^2\omega'^2 + \Delta(k',i\omega')^2 + \hbar^2\upsilon_F^2(k'-k_F)^2}\,. \tag{2}$$

In Ref. 9, dynamic screening effects have been considered in the excitonic state accounting for the fact that electron and holes bound as condensed excitons cannot screen as efficiently as free carriers (they can do so only by

polarization at wavelengths smaller than their size), so that the dynamic polarizability $\Pi_\Delta(q, i\omega)$ calculated self-consistently in the superfluid state should be employed to obtain an interaction potential $eV_\Delta^{(\mathrm{RPA})}(\boldsymbol{q}, i\omega)$ in Eq. (2). Given the critique of Ref. 10, in the following, attention will be paid mainly to the unscreened potential. Nevertheless, comparison with results obtained using static and dynamic screening in the normal state will be made occasionally in order to emphasize the fact that the "unscreened" results presented here constitute a very generous upper bound to the gap.

B. Weak-coupling limit

Well-known estimates for the gap can be obtained in the weak coupling limit:[3,7,29] When $\Delta(k_\mathrm{F}) \ll E_F$, the integrand of Eq. (1) is strongly peaked at $k \sim k_\mathrm{F}$, so it is possible to use solve Eq. (1) in its linearized form obtaining:

$$\Delta(k_\mathrm{F}) \approx 2\delta_\mathrm{c} E_F \exp\left(-\frac{1}{\nu e V_\mathrm{eff}}\right), \tag{3}$$

where $\nu = E_F/(2\pi\hbar^2 v_\mathrm{F}^2)$ is the density of states at the Fermi surface and

$$V_\mathrm{eff} = \int_0^\pi \frac{\mathrm{d}\phi}{\pi} \frac{1+\cos\phi}{2} V^{(\mathrm{RPA})}\left(2k_\mathrm{F}\cos\frac{\phi}{2}, 0\right). \tag{4}$$

In the same limit, the critical temperature can be obtained in a standard way by going back to the finite-temperature expression for the gap:[7,12,29]

$$k_\mathrm{B}T_c \approx \frac{e^\gamma}{\pi} 2\delta_\mathrm{c} E_F \exp\left(-\frac{1}{\nu e V_\mathrm{eff}}\right) \approx 0.567\,\Delta(k_\mathrm{F}), \tag{5}$$

where $\gamma \approx 0.577$ is Euler's constant. In Eq. (3), δ_c is a cutoff of the order of unity discussed in Ref. 29 in general and in Ref. 3 in the specific case of interest here. Kharitonov and Efetov[7] have provided estimates for the effect of static screening on the gap: In the absence of any gate and with the bilayer surrounded by a homogeneous dielectric, indicating with $\eta_\mathrm{v} = \eta_\mathrm{s} = 2$ the valley and spin degeneracy, $V^{\mathrm{RPA}}(\boldsymbol{q}) \sim e/[2\epsilon(q+2\kappa)] < e/(4\epsilon\kappa)$ with $\kappa = e^2\Pi/(2\epsilon) = e^2\nu\eta_\mathrm{v}\eta_\mathrm{s}/(2\epsilon)$ (see Eq. (10)), where Π is the long-wavelength limit of the static polarizability of a graphene single-layer (see Eq. (11) below). Therefore $\nu e V_\mathrm{eff} \approx 1/(2\eta_\mathrm{v}\eta_\mathrm{s})$, and, accounting for a factor of 2 resulting from the integration of the chiral factor $(1+\cos\phi)/2$ over ϕ, $\Delta(k_\mathrm{F}) \sim 2\delta_\mathrm{c}E_F e^{-4\eta_\mathrm{v}\eta_\mathrm{s}} \approx 2\delta_\mathrm{c}E_F e^{-16} \approx 10^{-7} 2\delta_\mathrm{c}E_F$. These estimates show how dramatically static screening can affect the superfluid gap, especially considering that they constitute strict and optimistic upper bounds obtained assuming a vanishing interlayer separation and ignoring the q dependence of the potential.

C. Some simple examples

Typical results for the gap $\Delta(k)$ are shown in Figs. 1 and 2: The first figure shows the gap for various values of the Fermi energy (assuming perfect charge balance in the BLG) using the bare interlayer potential $e^2(2\epsilon q)e^{-qd}$ (a) assuming air gaps $(\epsilon/\epsilon_0 = \kappa = 1)$ or the potential derived in Sec. III below for a very remote gate ((b), gate insulator thickness of 100 nm) and $\kappa = 3.9$ throughout. As predicted originally,[1–3] gaps of the order of E_F are observed at a sufficiently high carrier density. On the contrary, the RPA-like-screened potential (using the polarizability of SLG from Refs. 30 and 31) yields a gap orders of magnitude smaller (Fig. 2 to be compared to Fig. 1(b)), consistent with the estimates provided by Eq. (3) above. The dependence of $\Delta(k)$ on E_F is shown in Fig. 3 ((a) unscreened potential; (b) screened potential). Note how in the unscreened case the gap increases monotonically with Fermi energy while screening suppresses the interaction at sufficiently high densities, as already remarked by Abergel *et al.*[10,12]

III. POTENTIAL FOR GATED BILAYERS

In this section, the ideal geometry of a BLG suspended in a homogeneous dielectric is replaced by the more realistic geometry of a gated BLG in a heterogeneous medium. The geometry considered here consists of graphene bilayers on the (x,y) plane with the two SLGs at $z = 0$ and $z = d$, an ideal metal filling the half-space $z < -t'$, an ideal metal filling the half-space $z > d + t$, a substrate dielectric with dielectric constant ϵ_s filling the bottom gate-insulator region $-t' \le z < 0$, a dielectric with dielectric constant ϵ_i in $0 \le z < d$, and a gate dielectric with dielectric constant ϵ_g in the region $d \le z < d + t$. The bottom and top metals are

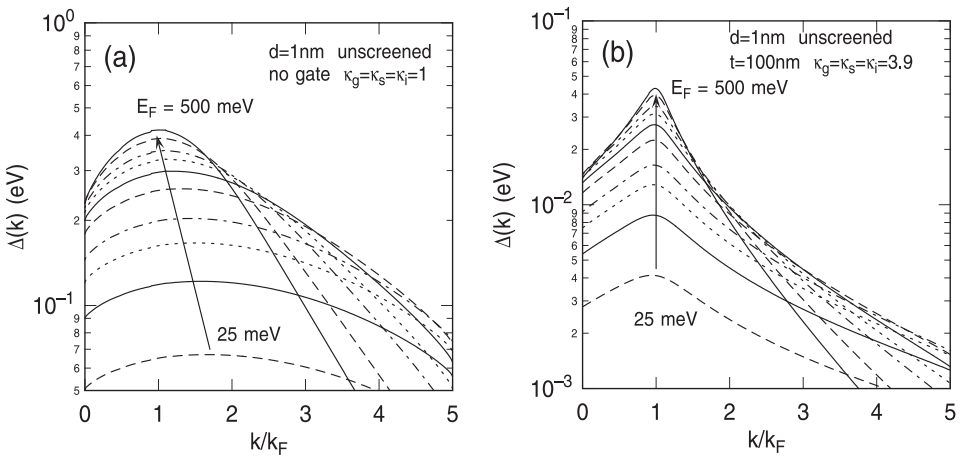

FIG. 1. (a) Calculated dependence of the superfluid gap Δ on wave vector k for a BLG in air with layers separated by a distance $d = 1$ nm and using the bare interlayer potential with Fourier components $e^2/(2\epsilon_0 q)\exp(-qd)$. The curves are labeled by the value of the Fermi energy $E_\mathrm{F} = 500$, 400, 300, 250, 200, 150, 100, 75, 50, and 25 meV. (b) As in (a), but assuming the BLG embedded in a dielectric medium with dielectric constant $\epsilon = 3.9\ \epsilon_0$ and assuming a metallic gate with a gate insulator thickness t of 100 nm, sufficiently remote to have any significant effect.

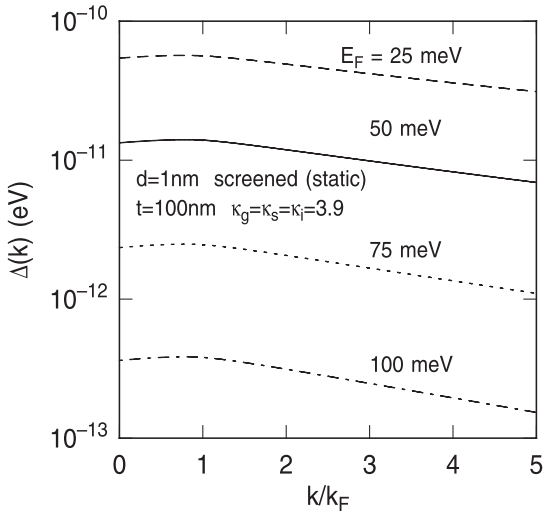

FIG. 2. As in Fig. 1(b), but using now the statically screened interlayer potential. Note the dramatic reduction of the gap, consistent with the estimate given by Eq. (3). The values of the gap for E_F larger than 100 meV are too small to be shown, as seen in Fig. 3(b).

assumed to be "ideal" in the sense that at the wavelengths and frequencies considered here (smaller than the screening wave vector $[e^2mk_F/(\pi^2\hbar^2\epsilon_0)]^{1/2}$ (~10–30/nm for a carrier density $n \sim 10^{22} - 10^{23}\,\mathrm{cm}^{-3}$ and a free electron mass m) and than the plasma frequency $\omega_P = [e^2n/(\epsilon_0 m)]^{1/2} \sim 6 \times 10^{15} - 10^{16}/\mathrm{s} \sim 10$ eV, respectively) it is appropriate to assume an infinite (negative) dielectric constant and so a vanishing potential in the regions $z < -t'$ and $z > d + t$. The frequency dependence of the dielectrics is also ignored for now but will be briefly considered in Sec. IV C 2 below. The relative dielectric constants ϵ/ϵ_0, where ϵ_0 is the vacuum permittivity, are denoted by κ. The physical and dielectric thickness of the insulators and their dielectric constants considered here span a wide range of values in order to study the problem "in principle." The realistic range of values, especially those pertinent to the BiSFET design, is considered in Refs. 13 and 14 and will be implicit in the discussion of the results presented below.

A. Poisson Green's function

For this geometry, the Green's function $g(q;z,z')$ for $z' \in (0,d)$ has the form

$$g(q;z,z') = \begin{cases} 0 & (z < -t') \\ a_0(q)e^{qz} + a_1(q)e^{-qz} & (-t' \le z < 0) \\ a_2(q)e^{qz} + a_3(q)e^{-qz} & (0 \le z < z') \\ a_4(q)e^{qz} + a_5(q)e^{-qz} & (z' \le z < d) \\ a_6(q)e^{qz} + a_7(q)e^{-qz} & (d \le z < t+d) \\ 0 & (t+d \le z) \end{cases}, \tag{6}$$

with coefficients $a_i(q)$, $(i = 0, 7)$ given by

$$\begin{aligned} a_0(q) &= \frac{2\epsilon_i}{\epsilon_s\gamma_+(q) - \epsilon_i\gamma_-(q)E(q)} \\ &\quad \times \frac{F(q)e^{qz'}}{q\{1 + F(q) - e^{2qz'}[1 - F(q)]\}} \\ a_1(q) &= -a_0(q)e^{-2qt'} \\ a_2(q) &= \frac{a_0(q)\gamma_-(q)q[1 - F(q)] + F(q)e^{qz'}}{q\{1 + F(q) - e^{2qz'}[1 - F(q)]\}} \\ a_3(q) &= -e^{qz'}\frac{a_0(q)\gamma_-(q)qe^{qz}[1 - F(q)] + F(q)}{q\{1 + F(q) - e^{2qz'}[1 - F(q)]\}} \\ a_4(q) &= \frac{a_2(q) - a_3(q)e^{-2qz'} - e^{-qz}/q}{1 + e^{2q(d-z')}H(q)} \\ a_5(q) &= -a_4(q)e^{2qd}H(q) \\ a_6(q) &= \frac{\epsilon_i}{\epsilon_g}\frac{a_4(q) - a_5(q)e^{-2qd}}{1 + e^{2qt}} \\ a_7(q) &= -a_6(q)e^{2q(d+t)}, \end{aligned} \tag{7}$$

where $\gamma_\pm(q) = 1 \pm e^{-2qt'}$ and

$$\begin{aligned} H(q) &= \frac{\epsilon_d(1 + e^{2qt}) - \epsilon_i(1 - e^{2qt})}{\epsilon_d(1 + e^{2qt}) + \epsilon_i(1 - e^{2qt})} \\ F(q) &= \frac{1 - e^{2q(d-z')}H(q)}{1 + e^{2q(d-z')}H(q)} \\ E(q) &= \frac{1 + F(q) + e^{2qz'}[1 - F(q)]}{1 + F(q) - e^{2qz'}[1 - F(q)]} \end{aligned} \tag{8}$$

In terms of these Fourier components of the Green's function, the in-plane Fourier components of the electrostatic potential due to a charge e at $\boldsymbol{r}' = (\boldsymbol{R}', z')$ will be $V(q;z,z') = (e/\epsilon_i)g(q;z,z')$. The limit $t' \to \infty$ corresponds

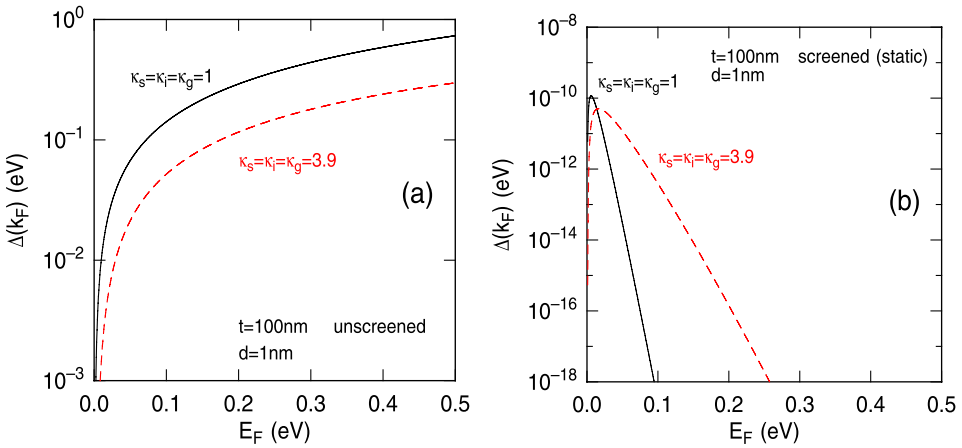

FIG. 3. Dependence of the superfluid gap at the Fermi surface, $\Delta(k_F)$, on Fermi energy for a BLG embedded in air (solid line) or a medium with relative dielectric constant $\kappa = 3.9$ (dashed line) calculated assuming the unscreened (a) or screened (b) interlayer potential. The distance between the SLGs is assumed to be 1 nm and the metallic gate is assumed to be too far ($t = 100$ nm) to matter. The results shown here are obtained from Eq. (3) with $\delta_c = 1$.

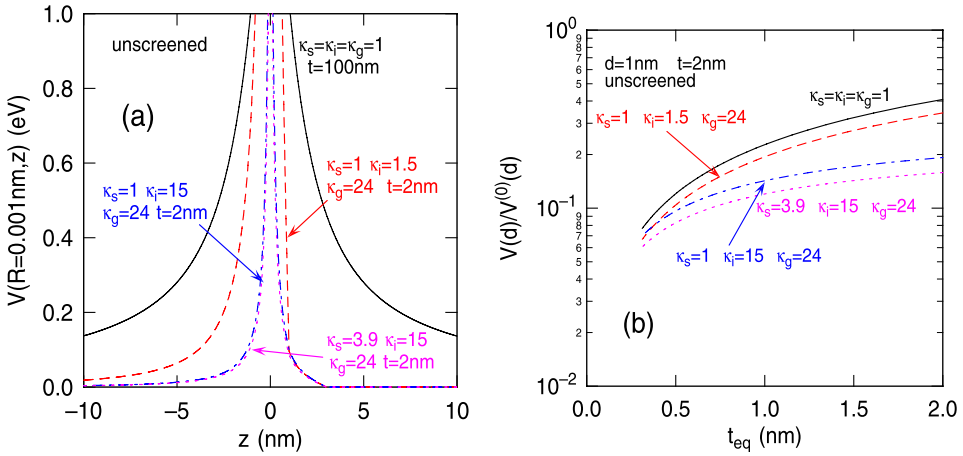

FIG. 4. (a) Total electrostatic potential in BLG with interlayer distance $d=1$ nm due to a charge e located at $z=0^+$. In order to avoid the singularity, the potential is plotted at the very small in-plane distance of 0.001 nm away from the charge. Four different dielectric geometries are illustrated: 1. A "benchmark" geometry of a BLG suspended in air with a gate 100 nm above the top SLG (solid line); 2. The same, but now with a reduced gate-insulator thickness ($t=2$ nm), a high-κ (24, as for HfO_2) gate dielectric and a low-κ ($\kappa=1.5$) interlayer dielectric (dashed line); 3. As in the previous case, but with a higher-κ interlayer dielectric (15, as for Al_2O_3); 4. As in the previous case, but now replacing the air substrate with a dielectric with $\kappa=3.9$ (as for SiO_2 or hBN). Note that as soon as a nearby gate is introduced, the magnitude of the electrostatic potential at $z=d$ is dramatically reduced. (b) Calculated electrostatic potential at $z=d$ as a function of equivalent oxide thickness for the 4 dielectric geometries used in (a) and a physical gate-insulator thickness of 2 nm. The potential is normalized to the "un-gated" value $e^2/(4\pi\epsilon_0 d)$. In comparing cases 2 ($\kappa_i=1.5$) and 3 ($\kappa_i=15$), notice how a higher-κ interlayer dielectric actually results in a stronger interaction when an even higher-κ gate insulator is present, since a larger dielectric discontinuity results in stronger screening via interface polarization charges.

to the case of a single gate at a distance t from the top SLG, and this limit is employed in the following with the exception of the final discussion in Sec. IV C.

Figure 4(a) shows the total potential $(e/\epsilon_i\Omega)\sum_{\boldsymbol{q}} g(q;z,z')e^{i\boldsymbol{q}\cdot\boldsymbol{R}}$ calculated at $(\boldsymbol{R},z)$ with $R=0.001$ nm for a charge e at $(\boldsymbol{R}'=0,z'=0^+)$ for the various dielectric combinations indicated in the legend of that figure and for a gate/top SLG distance of $t=2$ nm. Frame (b) of the same figure shows the dependence of the interaction potential (normalized to the potential obtained in the absence of a gate for a BLG in air) on the distance to the gate expressed in terms of the equivalent SiO_2 thickness, t_{eq} when varying κ_g for a fixed physical gate-oxide thickness t (=2 nm). Note the strong effect of the gate in depressing the interaction potential at $z=d$. Since in the weak-coupling limit the superfluid gap depends exponentially on this potential via Eq. (3), it is easy to understand why an ideal-metal gate can have such a strong effect on the gap itself, as shown below.

B. Dielectric screening

The screened (in the normal state) potentials $V^{(\mathrm{RPA})}(q,i\omega;0)$ and $V^{(\mathrm{RPA})}(q,i\omega;d)$ at $z=0$ and $z=d$, respectively, due to a charge at $z'=0^+$ can be obtained using the RPA-like approximation following the arguments given by Kharitonov and Efetov,[7] obtaining

$$\begin{aligned} V^{(RPA)}&(q,i\omega;d) \\ &= V(q;d)\{[1-(e^2/\epsilon_i)g(q;d,d)\,\Pi_d(q,i\omega)] \\ &\quad\times[1-(e^2/\epsilon_i)g(q;0,0)\,\Pi_0(q,i\omega)] \\ &\quad-(e^2/\epsilon_i)^2 g(q;0,d)^2\,\Pi_0(q,i\omega)\,\Pi_d(q,i\omega)\}^{-1}, \end{aligned} \tag{9}$$

where $\Pi_0(q,i\omega)$ and $\Pi_d(q,i\omega)$ are the dynamic polarizabilities of the SLG at $z=0$ and $z=d$, respectively, polarizabilities that may differ in principle. In deriving this expression, it should be noted that $V(q;0)=(e/\epsilon_i)g(q;0,0)$, $V(q;d)=(e/\epsilon_i)g(q;d,0)$, and that $g_q(z,z')=g_q(z',z)$. Note that in absence of any gate, assuming that the bilayer is surrounded by a homogeneous dielectric medium of dielectric constant ϵ, and considering the static limit and the optimal case of equal densities in the two layers so that $\Pi_0(q,i\omega=0)=\Pi_d(q,i\omega=0)=\Pi(q)$, this expression reduces to the well-known form

$$V^{(RPA)}(q,0;d) = \frac{e}{2\epsilon}\frac{e^{-qd}}{q-2\kappa+\kappa^2(1-e^{-2qd})/q}, \tag{10}$$

having set $v(q)=V(q,0)=e/(2\epsilon q)$ and $\kappa=eqv(q)\Pi(q)$, following Ref. 7. Figure 5(a) illustrates the dependence of the statically screened interaction potential on charge density for the same combinations of dielectrics employed in Fig. 4. Frame (b) of the figure shows the dependence of the screened potential on t_{eq}, as in Fig. 4(b).

IV. RESULTS AND DISCUSSION

A. Single-gate geometry

In order to assess how the proximity of a metallic gate affects the magnitude of the gap, Eq. (1) is solved by iteration starting from a Lorentzian initial guess of height 0.025 eV and half-width 0.01 k_F and using either the unscreened potential given by Eq. (6) with the coefficients given by Eq. (7) or the statically screened potential, Eq. (9). The integration over the angle ϕ is performed employing 180 intervals in $(0,\pi)$ while the integration over the magnitude of $\boldsymbol{k}$ is performed employing a non-uniform mesh consisting of three intervals: A first interval $[0,(1-\delta)k_F]$ divided uniformly into 100 elements, an interval $[(1-\delta)k_F,(1+\delta)k_F]$ in which the integration can be performed

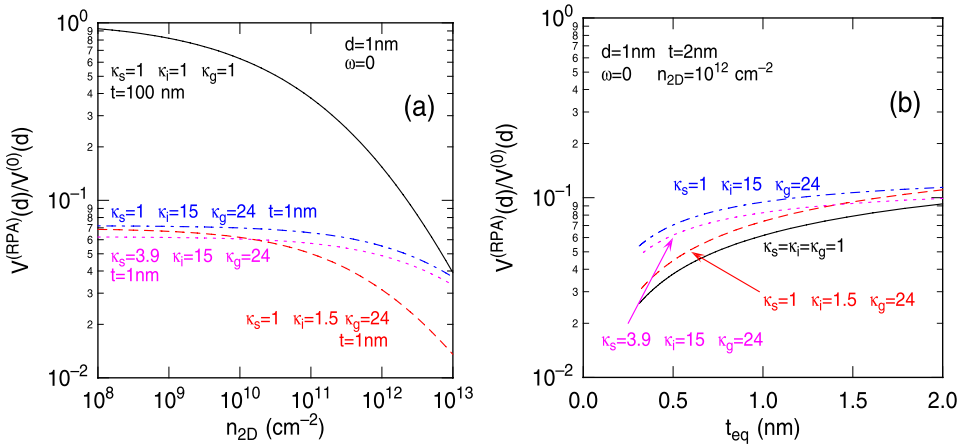

FIG. 5. Calculated value of the interlayer potential as in Fig. 4(a) but now statically screened and plotted as a function of charge density in the layers (a) and equivalent oxide thickness (b). The potential is normalized to the value in the un-gated, unscreened case with BLG in air. Note in the (b) how a small dielectric mismatch is preferable in the presence of a high-κ gate insulator.

analytically as done to obtain Eq. (3), and a third interval $[(1+\delta)k_F, k_{max}]$ uniformly divided into ~1000 elements. The cutoff parameter δ is set to 0.05–0.1 after some numerical experiments aimed at avoiding numerical artifacts due to this choice. The short-wavelength cutoff k_{max} is set to 10-to-50 k_F. Convergence—established when both the root-mean-square and the maximum relative error are smaller than 10^{-4}—is usually reached in 10–50 iterations, depending on the final magnitude of $\Delta(k_F)$, smaller magnitudes requiring a larger number of iterations. In some cases, such as for screened interactions with large dielectric constants and dielectric mismatches in the system, the iteration is halted before convergence is reached since the magnitude of $\Delta(k_F)$ reaches excessively small values with little or no physical meaning. In the strong-coupling limit (unscreened potential, low κ, large t), only the full solution of the integral Eq. (1) can provide a quantitatively correct the maximum value of the gap, usually close to (but not exactly *at*) k_F. In the weak-coupling limit (screened interaction, high-κ dielectrics, small t), the value of the gap $\Delta(k_F)$ obtained using Eq. (3) (with $\delta_c = 1$) is quantitatively close to the "exact" value obtained using Eq. (1) but not *identical*, because of dependence on the parameter δ_c. Therefore the results shown in Figs. 1–9, obtained using Eq. (1), are quantitatively correct within the approximations employed. On the contrary, the results shown in Figs. 3–10, obtained using Eq. (3), are quantitatively correct only up to a factor of the order of unity. As a comparison of the results shown in Figs. 6 and 3 illustrates, the proximity of a metallic gate strongly depresses the value of the gap, dramatically so when using the statically screened potential but also in the unscreened case. This is even more evident in Figs. 7 and 8 that constitute the main result of this work: Figure 7 illustrates the fact even in the unscreened case the gap is suppressed substantially as soon as a gate realistically close ($t_{eq} = 2$ nm (a) or 1 nm (b)) is present. Figure 8 quantifies this conclusion: For BLGs with substrate and interlayer dielectrics with $\kappa_s = \kappa_i = 1$ (frame (a), as for air gaps) and 3.9 (frame (b), as for SiO_2 or hBN), an equivalent oxide thickness of 2 nm or less, as required in realistic low-power device applications, reduces the superfluid gap to values of 10 meV (for $\kappa_s = \kappa_i = 1$) or 1 meV (for $\kappa_s = \kappa_i = 3.9$), and so to $T_c \sim 100$ K or 10 K even when using an air gap as gap insulator (that implies $t \sim 0.25$ nm and so unacceptable gate tunneling). Even the presence of gate insulators with a relatively low κ (such as ≈4 for hBN) depresses the gap even more to 1 meV or less. In particular, for $t_{eq} \approx 1$ nm, $\Delta(k_F) \sim 0.1$ meV, or $T_c \approx 1$ K *even assuming an air gap as gate insulator, a single top or bottom gate, and a completely unscreened interlayer Coulomb interaction*. This is the motivation behind the new device design mentioned above.[13,14]

Another interesting observation already made in connection with Figs. 4(b) and 5(b) is shown in Fig. 9: This figure shows the k-dependent gap $\Delta(k)$ calculated assuming fixed substrate and gate dielectrics with $\kappa_s = 4$ and $\kappa_g = 24$, respectively, and varying the dielectric constant of the

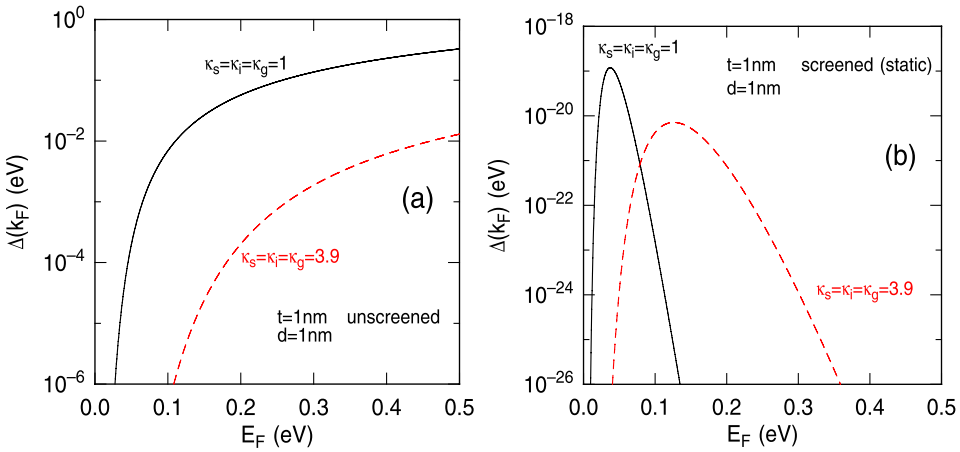

FIG. 6. As in Fig. 3 but for a nearby metallic gate, $t = 1$ nm instead of 100 nm. Note the significant reduction of the gap. As in Fig. 3, the results shown here are obtained from Eq. (3) with $\delta_c = 1$.

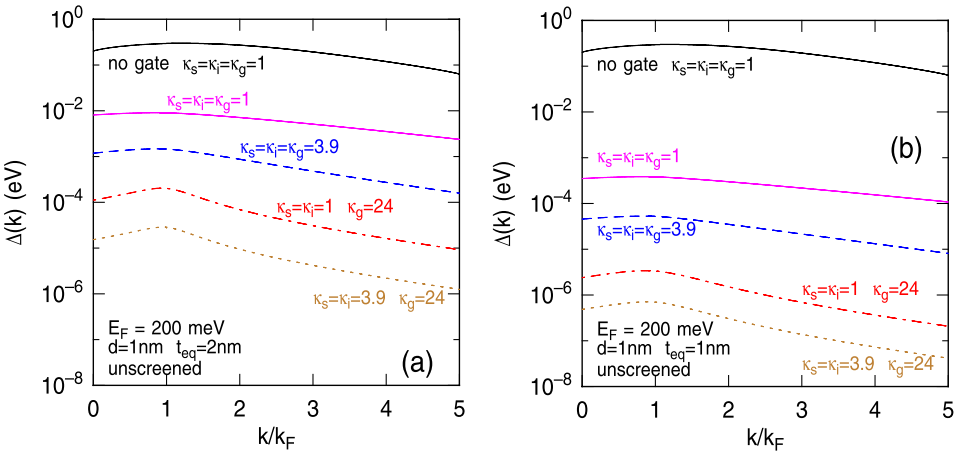

FIG. 7. Calculated superfluid gap as a function of wave vector employing the unscreened interlayer interaction and assuming the dielectric geometries shown in the legend assuming an equivalent oxide thickness of 2 nm (a) and 1 nm (b) and a Fermi energy of 200 meV.

interlayer insulator. The largest value of $\Delta(k_F)$ is obtained not for the smallest value of κ_i but for a value of $\approx$12 intermediate between 1 and $\kappa_g = 24$. A small value of κ_i induces a large dielectric mismatch that screens the attractive interlayer interaction while a larger value depresses it directly. This is consistent with Badalyan's and Peeters' results showing that approximating the effect of an inhomogeneous dielectric environment with an "average" dielectric constant may underestimate the strength of the inter-layer interaction.[19,20] Finally, Fig. 10 illustrates the dependence of the unscreened gap on physical insulator thickness (a) and interlayer separation (b). Clearly, at small interlayer separations (d smaller than about 1 nm), interlayer tunneling would dominate.

B. Double-gate geometry

A last important observation can be made about the effect of the proximity a second gate in double-gate (DG) configurations considered in device applications[13,14] and employed in Coulomb-drag experiments.[16] Figure 11 illustrates the dramatic reduction of the superfluid gap in DG structures as the dielectric constants of the gate insulators are increased for the two cases of an air (a) or SiO_2 (or hBN) interlayer dielectric (b). Comparing this figure to Fig. 8 (and keeping in mind the lower values of E_F adopted there), the much faster reduction of the gap with increasing $\kappa_g = \kappa_s$ should be noted, especially in the case $\kappa_i = 1$ that is affected by a larger dielectric mismatch. Low-κ ($\kappa \leq 2$) and thick ($t_{eq} \geq 7.5$-to-10 nm) gate insulators are required to obtain a room-temperature transition ($\Delta(k_F) \sim 10^{-2}$ eV) and, indeed, these design constrains have been being accounted for in Refs. 16 ($t_{eq} \geq 20$ nm and hBN insulators, $\kappa \approx 4$), 13, and 14 ($t_{eq} \geq 10$ nm and low-κ, $\kappa \approx 2$, gate insulators).

C. Dynamic screening in the normal state

It has been already mentioned that accounting correctly for the effects of dynamic dielectric screening in BLG is extremely difficult.[10] For this reason, so far, no attempts have been made in this article to provide definite estimates of its effect on the superfluid gap. However, at this point, it may be useful to estimate at least qualitatively the effects of dynamic screening, albeit only in the normal state, in order to show explicitly how the values of $\Delta(k_F)$ obtained here assuming an unscreened interaction constitute extremely optimistic (perhaps excessively so) upper bounds to the elusive "truth." In order to gain some qualitative insight on the possible effect of dynamic screening, it is convenient to look first at the dynamically screened potential. The dynamic SLG polarizability for real frequencies, $\Pi(q,\omega)$, has been calculated in Refs. 30 and 31. Its continuation to complex frequencies, $\Pi(q,i\omega)$, can be obtained from the expressions given in these references and can be recast in the form[32]

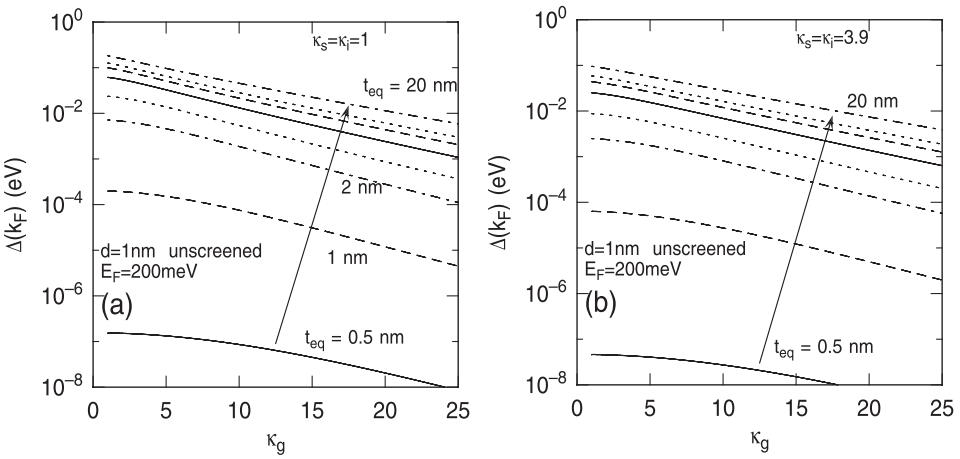

FIG. 8. Dependence of the calculated gap at the Fermi surface as in Fig. 7 on the dielectric constant κ_g of the gate insulator assuming $\kappa_s = \kappa_i = 1$ (a) or 3.9 (b). The curves are parametrized by the value of the equivalent oxide thickness of the gate insulator: $t_{eq} = 0.5$, 1, 2, 3, 5, 7.5, 10, and 20 nm. As in the previous figure, the calculations have been performed assuming a Fermi energy of 200 meV and, as in Fig. 3, the results shown here are obtained from Eq. (3) with $\delta_c = 1$.

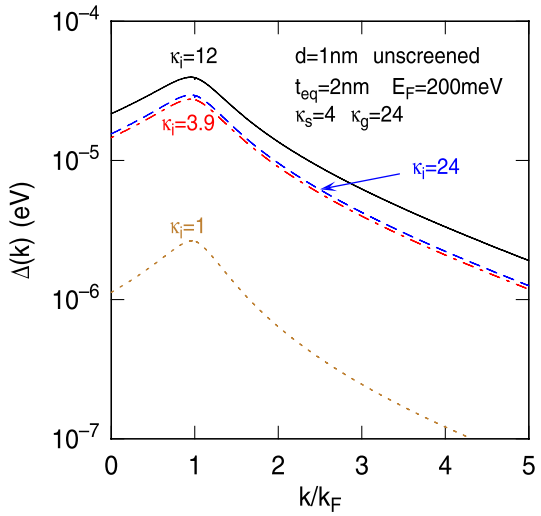

FIG. 9. Calculated gap Δ as a function of wave vector k assuming an unscreened interaction, a Fermi energy of 200 meV, an interlayer separation of 1 nm, an oxide-equivalent gate thickness $t_{eq} = 2$ nm, and substrate and gate relative dielectric constants $\kappa_s = 4$ and $\kappa_g = 24$, respectively. The four curves are labeled by the relative dielectric constants of the interlayer dielectric, $\kappa_i = 1$ (dotted line), 3.9 (dash-dotted line), 12 (solid line), and 24 (dashed line). Note that in the presence of a high-κ gate insulator, a low-κ interlayer dielectric may actually be counterproductive, as already noted in Refs. 13 and 14. An optimum κ_i is seen at ≈12, since a larger value suppresses the direct attractive interlayer interaction, whereas a lower value induces a large interface polarization charge that screens the interaction.

$$\Pi(q,i\omega) = -\frac{\eta_v\eta_s q^2}{16\sqrt{\hbar^2\omega^2+\hbar^2 v_F^2 q^2}} - \frac{\eta_v\eta_s E_F}{2\pi\hbar^2 v_F^2} + \frac{\eta_v\eta_s q^2}{8\pi\sqrt{\hbar^2\omega^2+\hbar^2 v_F^2 q^2}}\,\mathrm{Re}\left[\mathrm{asin}(y) + y\sqrt{1-y^2}\right], \tag{11}$$

with $y = (2E_F + i\hbar\omega)/(\hbar v_F q)$. Figure 12 illustrates the dependence of the screened potential $V^{(RPA)}(q, z)$, on complex frequency (frame (a), $z = i\omega$) and real frequency (frame (b), $z = \omega$) plotted as a function of the variable $\nu = (\hbar|\omega|/E_F)/[1 + (\hbar|\omega|/E_F)]$, as done in Ref. 9. Note in (a) that the potential (normalized to the unscreened potential for an un-gated BLG in vacuum) remains essentially statically screened up to frequencies comparable to the Fermi energy. More interesting, in (b), the interaction potential becomes repulsive for $\omega_- < \omega < \omega_+$ when both plasmon singularities, $\omega_\pm(q)$, are present on the real axis. This occurs as long as the polarizability of SLG, $\Pi(q,\omega)$, is real, that is, for $q/k_F < \hbar\omega/E_F < 2 - q/k_F$. The dispersion of the plasmons, that exhibit even modes (for free carries in the layers oscillating in phase) and odd modes (out-of-phase oscillations), is given implicitly by $\Pi[q,\omega_\pm(q)] = (\epsilon_i/e^2)/[g_0(q) \pm g_d(q)]$, that is, by the roots of the denominator of Eq. (9) (see also Ref. 33 and Eq. (3) of Refs. 19 and 20),

$$1 - 2(e^2/\epsilon_i)g_0(q)\Pi(q,\omega) + (e^2/\epsilon_i)^2 \times [g_0(q)^2 - g_d(q)^2]\Pi(q,\omega)^2 = 0, \tag{12}$$

having set $g(q;0,0) = g(q;d,d) = g_0(q)$, $g(q;0,d) = g(q;d,0) = g_d(q)$, and $\Pi_0(q,\omega) = \Pi_d(q,\omega) = \Pi(q,\omega)$. So, while at large frequencies, the interaction potential approaches the unscreened value, at lower frequencies, dynamic effects are either not significant or even counter-productive when the response of BLG plasmons lags so much as to change the sign of the interaction. At the highest frequencies at which dynamic screening could be beneficial, the denominator of Eq. (2), or Eq. (13) below, becomes increasingly larger, so the effects of dynamic screening *per se*, important in the small-frequency range $\hbar\omega \sim \Delta(k_F)$, are indeed expected to increase the magnitude of the gap above its statically screened value, but not all the way to its unscreened strength, as remarked already by Abergel *et al.*[10] The role played by dynamic dielectric screening at a finite temperature in enhancing the strength of the inter-layer interaction has been considered also by Badalyan and Peeters who have looked at this interaction as a plasmon-mediated process in the context of the Coulomb-drag resistance.[19,20]

An expression for the gap assuming a dynamically screened interaction can be formulated in terms of the temperature (Matsubara) Green's functions as[34]

$$\Delta(k) = k_B T \sum_{n=-\infty}^{\infty} \int \frac{d\boldsymbol{k}'}{(2\pi)^2}\,\frac{1+\cos\phi}{2} \times \frac{\Delta(k',\,\omega_n)\, eV^{(RPA)}(|\boldsymbol{k}-\boldsymbol{k}'|, i\omega_n)}{\hbar^2\omega_n^2 + \Delta(k')^2 + \hbar^2 v_F^2 (k'-k_F)^2}, \tag{13}$$

where $\hbar\omega_n = \pi k_B T(2n+1)$ are the fermionic Matsubara frequencies and the frequency dependence of the gap has been neglected by taking its static value, as justified in Ref. 9. For

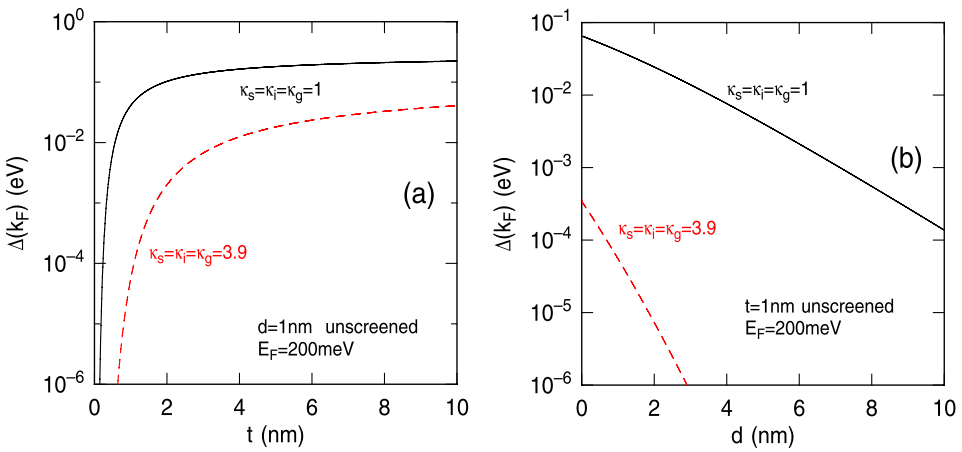

FIG. 10. Dependence of the calculated superfluid gap at the Fermi surface on physical gate-insulator thickness t (a) and interlayer separation d (b) assuming the dielectric geometries indicated, a Fermi energy of 200 meV, and an unscreened interlayer interaction. Since interlayer tunneling is ignored, small values of d represent an unrealistically idealized situation. As in Fig. 3 the results shown here are obtained from Eq. (3) with $\delta_c = 1$.

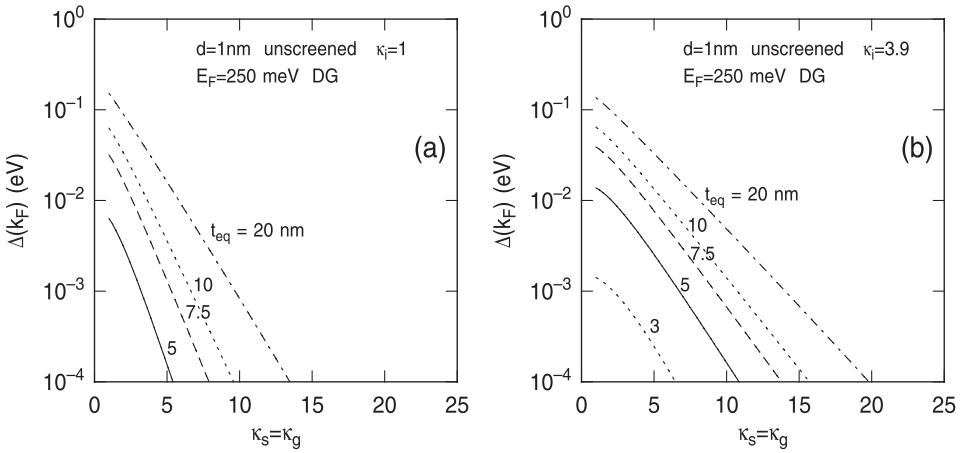

FIG. 11. Dependence of the calculated superfluid gap at the Fermi surface on the relative dielectric constant $\kappa_g = \kappa_s$ of the top- and bottom-gate dielectrics for a fully symmetric double-gate geometry. An interlayer dielectric with dielectric constant $\kappa_i = 1$ (a) and 3.9 (b) is assumed. The curves are parametrized by the equivalent oxide thickness over the range $t_{eq} = 20$, 10, 7.5, 5, and 3 nm. A Fermi energy of 250 meV and an unscreened interlayer interaction is also assumed. As in Fig. 3, the results shown here are obtained from Eq. (3) with $\delta_c = 1$.

a statically screened interaction, this equation reduces to the usual equation for the gap at a finite temperature since,

$$k_B T \sum_{n=-\infty}^{\infty} \frac{1}{\hbar^2\omega_n^2 + x^2} = \frac{1}{2x}\tanh\left(\frac{x}{2k_B T}\right). \tag{14}$$

In the limit $T \to 0$, the sum over the Matsubara frequencies can be converted into an integral, and the equation for the zero-T gap becomes

$$\Delta(k) = \int_0^{\infty} \frac{d(\hbar\omega)}{\pi} \int \frac{d\boldsymbol{k}'}{(2\pi)^2} \frac{1+\cos\phi}{2} \times \frac{\Delta(k')\, eV^{(RPA)}(|\boldsymbol{k}-\boldsymbol{k}'|, i\omega)}{\hbar^2\omega^2 + \Delta(k')^2 + \hbar^2 v_F^2 (k'-k_F)^2} \tag{15}$$

which is Eq. (14) of Ref. 9 with the dependence of Δ on k retained in the denominator.

1. Static response of the insulators

This equation is solved iteratively using the initial guess and discretization of the integrals over ϕ and k' described at the beginning of Sec. IV A, about 200 intervals up to $\hbar\omega = 10\,E_F$ for the integration over ω and with $\delta \approx 0.1$. Care must be taken since the contribution to the integral over k' arising from integration in the k'-interval $\mathcal{I}_F = [(1-\delta)k_F, (1+\delta)k_F]$ centered around the Fermi energy can be numerically troublesome around k_F in the weak-coupling and small-ω limits. Thus, for small $\Delta(k_F)$, an analytic integration is performed in the spirit of the approach followed to reach Eq. (3).

The resulting dynamically screened (in the normal state) value of the gap $\Delta(k_F)$ as a function of Fermi energy is shown in Fig. 13 for the case of a double-gated BLG with an interlayer air gap and top and bottom gate insulators with static dielectric constants $\kappa = 2$ and physical thickness $t = 5$ nm. Note that, while boosting the magnitude gap from its statically screened value, dynamic screening fails to recover the "unscreened" value.

2. Dynamic response of the insulators

A final observation can be made about the dielectric response of the insulators. In Ref. 13, it was tentatively suggested that the high-frequency dielectric constant should be employed. This may be the case if the frequency associated to the energy exchanged in the interlayer electron-hole interaction, $\sim\Delta(k_F)/\hbar$, was larger than the frequency of the insulator(s) optical phonons, ω_{TO}. However, the results presented so far show that as soon as high-κ dielectrics (with low $\hbar\omega_{TO}$ in

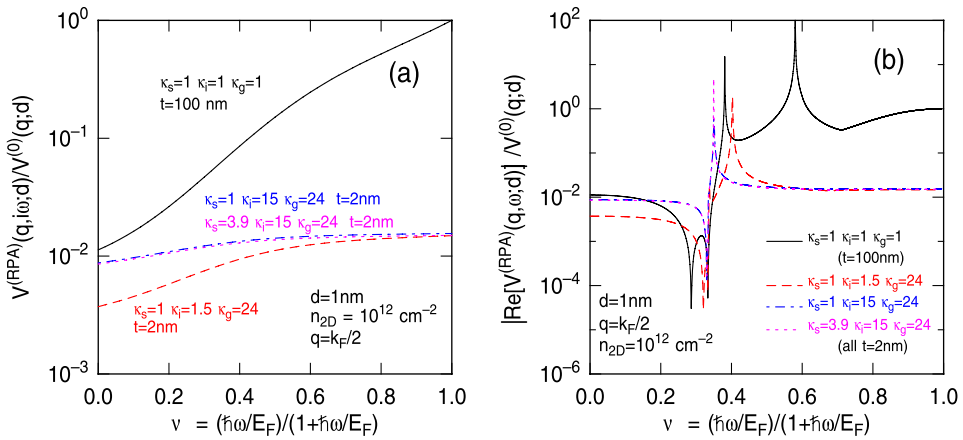

FIG. 12. Fourier components of the interaction potential calculated using the dynamic polarizability of SLG for complex (a) and real frequencies (b) for the four different dielectric geometries considered in previous figures assuming $q = k_F/4$ and a density $n_{2D} = 10^{12}$ cm^{-2}. In both cases, the potential is shown normalized to the un-gated, bare potential for BLG in vacuum. An interlayer distance $d = 1$ nm is assumed. Note that frame (b) shows the absolute value of the real part of the potential. The plasmon singularities $\omega_\pm$ are present only when $q/k_F < \hbar\omega < 2 - q/k_F$). When both plasmons are undamped, the potential becomes purely real and negative (repulsive) for $\omega_- < \omega < \omega_+$, so that dynamic screening may actually depress the gap.

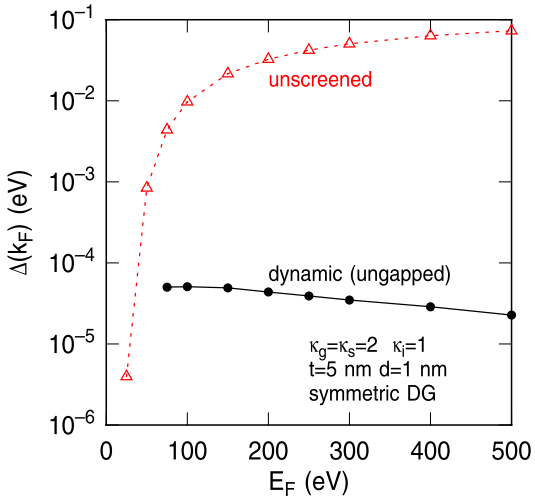

FIG. 13. Calculated dependence of the gap at the Fermi surface, $\Delta(k_F)$, on E_F itself for a symmetric double-gate BLG with $\kappa_i = 1$, $\kappa_s = \kappa_g = 2$ and a physical thickness t of 5 nm ($t_{eq} \approx 10$ nm). Note that un-gapped, dynamic screening still fails to boost the transition temperature to the value obtained assuming an unscreened inter-layer interaction. The values of $\Delta(k_F)$ for the statically screened case are too small to show. The lines connecting the symbols are just a guide to the eye.

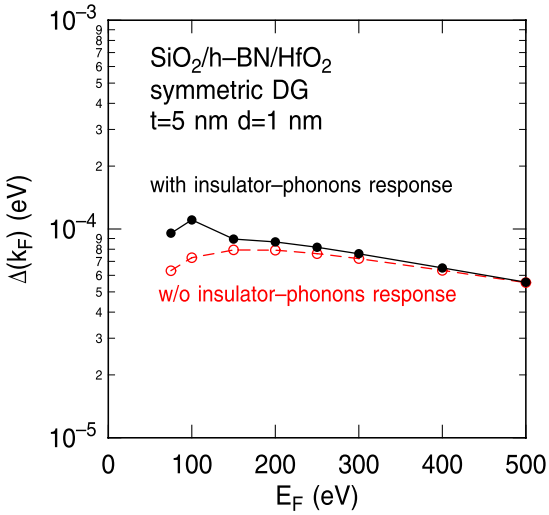

FIG. 14. Calculated dependence of the gap at the Fermi surface, $\Delta(k_F)$, on E_F itself for a double-gate BLG with SiO_2, hBN, and HfO_2 as bottom-gate, inter-layer, and top-gate insulators, respectively. HfO_2 has been chosen as top-gate dielectrics to emphasize the possible ionic frequency response of insulator optical phonons, thanks to the low frequency of its optical modes. Despite this choice, the modifications of the gap due to the response of the dielectrics are minor. The lines connecting the symbols are just a guide to the eye.

the range of 10 meV) are introduced, $\Delta(k_F)$ is reduced to much smaller values. Therefore, the use of the static dielectric constant seems more appropriate. In order to quantify this expectation, the dynamically screened gap has been evaluated by solving Eq. (15) with the dynamically screened interaction potential $eV^{(RPA)}(q, i\omega)$, Eq. (9) now calculated using the dynamic Poisson Green's function, $g(q, i\omega; z, z')$, given by Eqs. (6) and (7) with ϵ_s, ϵ_i, and ϵ_g replaced by their long-wavelength frequency dependent expressions reflecting the ionic response of the dielectrics. The specific case has been considered of a double-gate BLG with interlayer separation $d = 1$ nm, bottom and top gates $t = 5$ nm thick, and SiO_2, hexagonal BN (hBN), and HfO_2 as bottom-gate, interlayer, and top-gate insulators, respectively. The insulator dielectric functions $\epsilon_{s,i,g}(i\omega)$ have been calculated using the expression and parameters given in Ref. 35 for SiO_2 and HfO_2, obviously rotated to the imaginary-ω axis. For hBN, a single optical phonon with $\hbar\omega_{TO} = 168$ meV and high- and low-frequency dielectric constants $\kappa_\infty = 4.10$ and $\kappa_0 = 4.95$ (along the c-axis of the hexagonal lattice) have been employed.[36] HfO_2 as top gate insulator has been chosen because its low-energy TO phonons may maximize dynamic screening effects. Yet, as expected, the value of the gap is largely insensitive to the dielectric response of the insulators. This is illustrated in Fig. 14 showing that the gap at the Fermi energy calculated using the full dynamically screened interlayer interaction including the dielectric response of the dielectrics ($\Delta(k_F) = 47.8\ \mu$eV) is no more than a factor of 2 larger than the gap calculated employing the interaction screened dynamically only by the graphene free-carries and using the low-frequency (static) dielectric constants of the insulators ($\Delta(k_F) = 36.1\ \mu$eV).

V. CONCLUSIONS

The main conclusion to be drawn from the discussion presented above is that in BLG the proximity of an ideal-metal gate affects the magnitude of the interlayer Coulomb interaction and so the superfluid gap and the normal-superfluid transition temperature. Even assuming an unscreened interaction potential, a gate-insulator equivalent-oxide thickness of 1 nm, as needed in device applications, implies a transition temperature of 1 K even under the most optimistic conditions. Indeed, modified designs of the BiSFET[13,14] have been proposed employing the thicker ($t_{eq} \approx 10$ nm) low-κ ($\approx$2) gate insulators required to form and maintain the superfluid state at room temperature. This is particularly important in double-gate structures. Moreover, as already hinted in Refs. 13 and 14, a strong dielectric mismatch has an even stronger negative effect. Assuming very optimistically that static screening results in a severe underestimation of the transition temperature, a homogeneous low-κ dielectric environment (ideally, air gaps), gate-insulator(s) thickness larger than about 10 nm, and gate contacts with a non ideal-metal behavior (such as not excessively heavily doped semiconductors) may be required to observe the normal-superfluid transition. But the required proximity of the gate renders vary challenging the use of the superfluid state in high-performance, low-power devices.

ACKNOWLEDGMENTS

It is a pleasure to acknowledge extremely informative discussions with professor Allan H. MacDonald regarding the role of dielectric screening in BLG and with professors Sanjay K. Banerjee and Frank L. Register regarding the design requirements of the BiSFETs. This work has been supported in part by Texas Instruments and by the Nanoelectronics Research Initiative's (NRI's) Southwest Academy of Nanoelectronics (SWAN).

[1]C.-H. Zhang and Y. N. Joglekar, Phys. Rev. B **77**, 233405 (2008).
[2]H. Min, R. Bistritzer, J.-J. Su, and A. H. MacDonald, Phys. Rev. B **78**, 121401 (2008).

[3]Yu. E. Lozovik and A. A. Sokolik, J. Phys. Conf. Ser. **129**, 012003 (2008).
[4]S. Banerjee, L. Register, E. Tutuc, D. Reddy, and A. H. MacDonald, IEEE Electron Device Lett. **30**, 158 (2009).
[5]M. Yu. Kharitonov and K. B. Efetov, Phys. Rev. B **78**, 241401 (2008).
[6]R. Bistritzer, H. Min, J.-J. Su, and A. H. MacDonald, e-print arXiv:0810.0331v1[cond-mat.mes-hall].
[7]M. Yu. Kharitonov and K. B. Efetov, Semicond. Sci. Technol. **25**, 034004 (2010).
[8]Y. E. Lozovik, S. L. Ogarkov, and A. A. Sokolk, Phys. Rev. B **86**, 045429 (2012).
[9]I. Sodemann, D. A. Pesin, and A. H. MacDonald, Phys. Rev. B **85**, 195136 (2012).
[10]D. S. L. Abergel, M. Rodriguez-Vega, E. Rossi, and S. Das Sarma, Phys. Rev. B **88**, 235402 (2013).
[11]S. Das Sarma, S. Adam, E. H. Hwang, and E. Rossi, Rev. Mod. Phys. **83**, 407 (2011).
[12]D. S. L. Abergel, R. Sansarma, and S. Das Sarma, Phys. Rev. B **86**, 161412 (2012).
[13]L. F. Register, X. Mou, D. Reddy, W. Jung, I. Sodemann, D. Pesin, A. Hassibi, A. H. MacDonald, and S. Banerjee, ECS Trans. **45**, 3–14 (2012).
[14]D. Reddy, L. F. Register, and S. K Banerjee, "Bilayer Pseudospin Field Effect Transistor (BiSFET)," in *CMOS and Beyond*, edited by T.-J. King Liu and K. Khun (Cambridge University Press, Cambridge, UK, 2014).
[15]S. Kim, I. Jo, J. Nah, Z. Yao, S. K. Banerjee, and E. Tutuc, Phys. Rev. B **83**, 161401 (2011).
[16]R. V. Gorbachev, A. K. Geim, M. I. Katsnelson, K. S. Novoselov, T. Tudorovski, I. V. Gregorieva, A. H. MacDonald, S. V. Morozov, K. Watanabe, T. Taniguchi, and L. A. Ponomarenko, Nat. Phys. **8**, 896 (2012).
[17]P. Jadaun, H. C. Prakash, L. F. Register, and S. K. Banerjee, J. Appl. Phys. **114**, 063702 (2013).
[18]M. T. Allen and A. Yacobi, "Quantum confinement and broken symmetry in suspended bilayer graphene," in *Nanoelectronics Research Initiative WebEx E-workshop*, 28 May, 2013.
[19]S. M. Badalyan and F. M. Peeters, Phys. Rev. B **85**, 195444 (2012).
[20]S. M. Badalyan and F. M. Peeters, Phys. Rev. B **86**, 121405 (2012).
[21]T. Stauber and G. Gomez Santos, Phys. Rev. B **85**, 075410 (2012).
[22]R. E. V. Profumo, R. Asgari, M. Polini, and A. H. MacDonald, Phys. Rev. B **85**, 085443 (2012).
[23]See http://www.itrs.net/ for International Technology Roadmap for Semiconductors (ITRS).
[24]A. Perali, D. Neilson, and A. R. Hamilton, Phys. Rev. Lett. **110**, 146803 (2013).
[25]J. Zhang and E. Rossi, Phys. Rev. Lett. **111**, 086804 (2013).
[26]S. Das Sarma, E. H. Hwang, and W.-K. Tse, Phys. Rev. B **75**, 121406(R) (2007).
[27]S. Das Sarma and E. H. Hwang, Phys. Rev. B **87**, 045425 (2013).
[28]P. E. Trevisanutto, C. Giorgetti, L. Reining, M. Ladisa, and V. Olevano, Phys. Rev. Lett. **101**, 226405 (2008).
[29]A. L. Fetter and J. D. Walecka, *Quantum Theory of Many-Particle Systems*, (Dover, New York, 2003), Chap. 13.
[30]B. Wunsch, T. Stauber, F. Sols, and F. Guinea, New J. Phys. **8**, 318 (2006).
[31]E. H. Hwang and S. Das Sarma, Phys. Rev. B **75**, 205418 (2007).
[32]Y. Barlas, "Role of electron-electron interactions in chiral 2DEGs," Ph.D. thesis (The University of Texas, Austin, 2008).
[33]R. Roldan and L. Brey, Phys. Rev. B **88**, 115420 (2013).
[34]This expression, leading to Eq. (15), is employed here only in order to draw an analogy with Ref. 9. However it should be stressed that the integrand of Eq. (13) is not a meromorphic function. Indeed, in addition to the "Matsubara poles," the dynamically screened potential $V^{(\mathrm{RPA})}(q,z)$ is not a holomorphic function of $z \in \mathbb{C}$ because, in addition to plasmon singularities (or singularities due to coupled optical-phonon/plasmon modes when accounting for the dielectric response of the insulators), the singularity $\sim 1/\sqrt{v_F^2 q^2 - \hbar^2 z^2}$ of the polarizability $\Pi(q,z)$ gives raise to a branch-cut connecting the points $\pm v_F q$ on the real axis. Therefore this Matsubara function cannot be trivially continued analytically to the real-ω axis to obtain the real-time self-energy initially considered in Ref. 9.
[35]M. V. Fischetti, D. A. Neumayer, and E. A. Cartier, J. Appl. Phys. **90**, 4587 (2001).
[36]Landolt-Börnstein, *Group IV Elements, IV-IV and III-V Compounds. Part A—Lattice Properties; Group III Condensed Matter* (Springer, 2001), Vol. 41A1a.